

Chemical Vapor Deposition Synthesis and Terahertz Photoconductivity of Low-Band-Gap $N = 9$ Armchair Graphene Nanoribbons

Zongping Chen,[†] Hai I. Wang,[‡] Joan Teyssandier,[§] Kunal S. Mali,[§] Tim Dumsclaff,[†] Ivan Ivanov,[†] Wen Zhang,[†] Pascal Ruffieux,^{||} Roman Fasel,^{||,⊥} Hans Joachim Räder,[†] Dmitry Turchinovich,[†] Steven De Feyter,[§] Xinliang Feng,[#] Mathias Kläui,[‡] Akimitsu Narita,^{*,†} Mischa Bonn,^{*,†} and Klaus Müllen^{*,†,∇}

[†]Max Planck Institute for Polymer Research, Ackermannweg 10, D-55128 Mainz, Germany

[‡]Institute of Physics, Johannes Gutenberg-University Mainz, Staudingerweg 7, 55128 Mainz, Germany

[§]Division of Molecular Imaging and Photonics, Department of Chemistry, KU Leuven, Celestijnenlaan 200 F, B-3001 Leuven, Belgium

^{||}Empa, Swiss Federal Laboratories for Materials Science and Technology, nanotech@surfaces Laboratory, 8600 Dübendorf, Switzerland

[⊥]Department of Chemistry and Biochemistry, University of Bern, 3012 Bern, Switzerland

[#]Center for Advancing Electronics Dresden and Department of Chemistry and Food Chemistry, Technische Universität Dresden, Mommsenstrasse 4, D-01062 Dresden, Germany

[∇]Institute of Physical Chemistry, Johannes Gutenberg-University Mainz, Duesbergweg 10-14, 55128 Mainz, Germany

Supporting Information

ABSTRACT: Recent advances in bottom-up synthesis of atomically defined graphene nanoribbons (GNRs) with various microstructures and properties have demonstrated their promise in electronic and optoelectronic devices. Here we synthesized $N = 9$ armchair graphene nanoribbons (9-AGNRs) with a low optical band gap of ~ 1.0 eV and extended absorption into the infrared range by an efficient chemical vapor deposition process. Time-resolved terahertz spectroscopy was employed to characterize the photoconductivity in 9-AGNRs and revealed their high intrinsic charge-carrier mobility of approximately $350 \text{ cm}^2 \cdot \text{V}^{-1} \cdot \text{s}^{-1}$.

Graphene nanoribbons (GNRs), quasi-one-dimensional graphene strips, have attracted much attention as a new class of semiconducting materials for various applications in electronic and optoelectronic devices.^{1–6} In the past few years, various types of GNRs have been synthesized via bottom-up approaches in solution as well as on metal surfaces^{3–11} with a wide range of band gap energies. Among the different bottom-up methods, on-surface synthesis, especially through chemical vapor deposition (CVD), appears to be highly promising, as it is capable of high-throughput and scalable growth of structurally defined GNRs at low cost.^{6,8,12} The surface-grown GNR films can be readily transferred onto arbitrary substrates, allowing for optical characterizations and device integration. To date, however, the performance of field-effect transistor (FET) devices fabricated with such GNRs has been compromised by a huge contact resistance,^{6,8,10,12,13} hampering investigations of their intrinsic electronic transport properties.

For efficient optoelectronic applications such as photovoltaics, GNRs with an optical band gap between 1.0 to 1.3 eV are fundamentally important and are expected to provide GNR-based devices approaching the Shockley–Queisser limit.¹⁴ Nevertheless, structurally well-defined GNRs with optical band gaps in this range still remain rather rare.⁵ The electronic structure of armchair GNRs (N -AGNRs) has been shown to be extremely sensitive to the ribbon width, and AGNRs can be divided into three subfamilies with atomic number $N = 3n$, $3n + 1$, or $3n + 2$ ($n = 1, 2, 3, \dots$). All three kinds of AGNRs are expected to be semiconducting, and the band gaps of AGNRs from different subfamilies with the same n vary as $3n + 2 < 3n < 3n + 1$.^{1,2} According to theoretical prediction by GW-BSE calculations, $N = 9$ armchair graphene nanoribbons (9-AGNRs) possess an optical band gap of ~ 1.0 eV,¹⁵ which was very recently corroborated by the solution-mediated synthesis reported by Dong and co-workers.¹⁶ On the other hand, Nakae and co-workers previously proposed a synthesis of 9-AGNRs by a low-pressure CVD method;¹² however, the observed optical band gap was larger, and unambiguous structural characterization has remained elusive.

Here we report an efficient CVD process for inexpensive high-throughput growth of structurally defined 9-AGNRs. The obtained 9-AGNRs exhibit a low optical band gap of ~ 1.0 eV with broad absorption up to ~ 1200 nm. Ultrafast optical pump–terahertz probe spectroscopy (OPTP) is for the first time applied to surface-synthesized GNRs, revealing the high intrinsic charge-carrier mobility of 9-AGNRs, i.e., $\sim 350 \text{ cm}^2 \cdot \text{V}^{-1} \cdot \text{s}^{-1}$, which reflects the high quality of the sample fabricated

Received: January 23, 2017

Published: March 1, 2017

by our CVD method. The potential of 9-AGNRs for future optoelectronics has been further demonstrated in comparison with previously reported 7-AGNRs and chevron-type GNRs, showing higher photoconductivity by factors of 1.2 and 2.5, respectively.

We recently reported the efficient ambient-pressure CVD growth of 7-AGNRs and chevron-type GNRs.⁶ Notably, the CVD-grown GNRs demonstrated structural perfection well comparable to that of GNRs synthesized under ultrahigh-vacuum conditions. Because of its high versatility, our CVD process provides access to a broad class of GNRs with designed structures by the use of different oligophenylene monomers. The synthesis of 9-AGNRs has been achieved by CVD using 3',6'-dibromo-1,1':2',1''-terphenyl (DBTP) as the monomeric building block (Figure 1). In a typical CVD experiment, DBTP

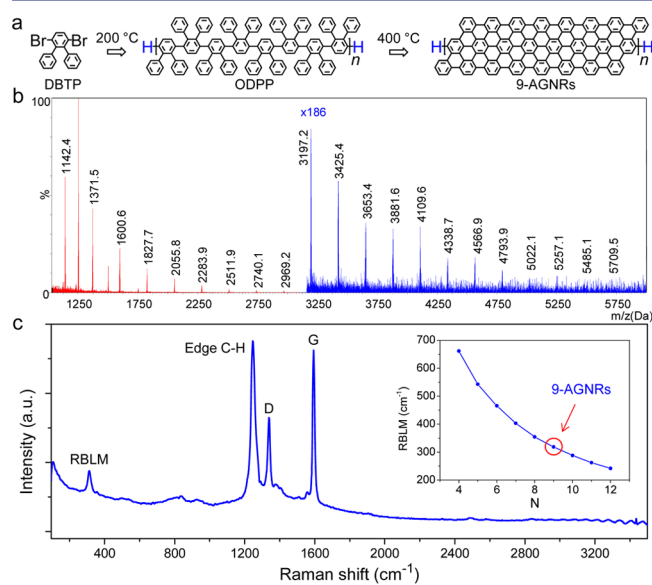


Figure 1. (a) Synthesis of 9-AGNRs by the CVD method. (b) Mass spectrum of ODPPs before cyclodehydrogenation. (c) Raman spectrum (785 nm laser) of CVD-grown 9-AGNRs. The inset shown the calculated RBLM peaks vs GNR width.¹⁷

is sublimed at 135–150 °C and deposited on a Au/mica substrate kept at 200 °C. At this temperature, DBTP is simultaneously dehalogenated, generating biradicals that subsequently undergo a coupling reaction to form oligo-(diphenyl-*p*-phenylene) (ODPP) with a linear backbone (Figure 1a). The sample is subsequently annealed at a higher temperature of 400 °C to transform ODPPs into 9-AGNRs through surface-assisted intramolecular cyclodehydrogenation, eliminating eight hydrogens per repeating unit.

To investigate the chemical structures of the oligomer/polymer after the radical polymerization step during the on-surface synthesis of GNRs, we recently developed a quick and powerful surface-mass-spectrometry analysis method.⁶ ODPPs were thus studied by high-resolution matrix-assisted laser desorption/ionization time-of-flight mass spectrometry (MALDI-TOF MS) with *trans*-2-[3-(4-*tert*-butylphenyl)-2-methyl-2-propenylidene]malononitrile (DCTB) as the matrix (Figure 1b). The MS spectrum of the ODPPs exhibits regular patterns from the pentamer ($m/z \approx 1142$ Da) up to a species with 23 units ($m/z \approx 5257$ Da). The difference between the neighboring signals is exactly the same value of ~ 228 Da, which corresponds to the molecular mass of the repeating unit. The

observed isotopic distribution of the ODPPs is in agreement with the simulated pattern, demonstrating the successful polymerization reaction to form the expected structures (Figure S1).

The Raman spectrum of the final 9-AGNRs after cyclodehydrogenation reveals four main peaks at 1592, 1340, 1250, and 315 cm⁻¹, which can be assigned to G, D, edge C–H, and radial breathing-like mode (RBLM) peaks, respectively (Figures 1c and S2).¹⁸ The sharp and intense width-specific RBLM peak is in excellent agreement with the DFT calculation, demonstrating the high uniformity in the width of the obtained 9-AGNR sample (inset of Figure 1c).¹⁷ It should be noted that the specific RBLM peak of 9-AGNRs was not observed in previous reports on 9-AGNRs obtained by CVD growth¹² and solution synthesis.¹⁶ The monolayers of as-synthesized 9-AGNRs were further unambiguously characterized using atomic force microscopy (AFM) as well as scanning tunneling microscopy (STM) under ambient conditions (Figures 2 and

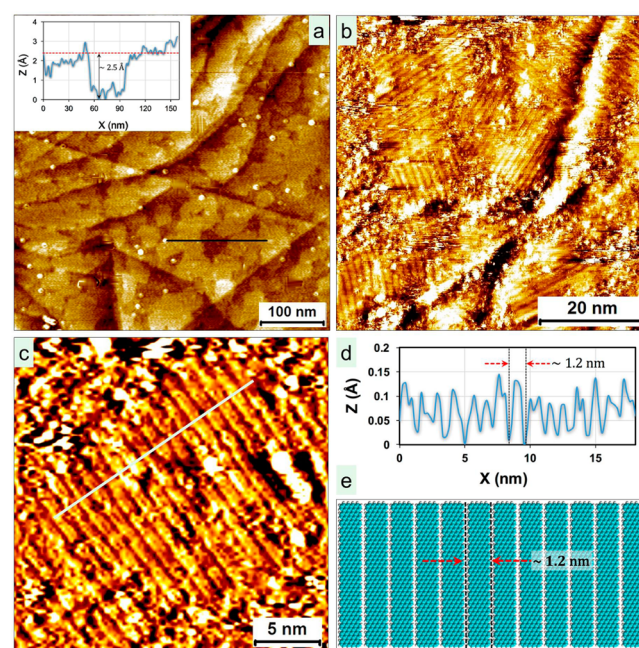


Figure 2. AFM/STM characterization of 9-AGNRs on a Au(111)/mica surface. (a) AFM height image showing domains of 9-AGNRs. The inset shows the height profile along the black line, indicating the formation of a monolayer of 9-AGNRs. (b) STM image showing domains of 9-AGNRs ($I_{\text{set}} = 300$ pA; $V_{\text{bias}} = 0.06$ V). (c) Small-scale STM image showing 9-AGNRs as well-defined stripes with uniform width of ~ 1.2 nm ($I_{\text{set}} = 60$ pA; $V_{\text{bias}} = 0.03$ V). (d) Line profile along the white line in (c). (e) Molecular model showing the laterally stacked 9-AGNRs.

S3). AFM height images show terraces of the Au(111) surface uniformly covered with a monolayer-thick (~ 2.5 Å) film of 9-AGNRs (Figure 2a). The STM images agree well with the AFM data, indicating good surface coverage of striped features (Figure 2b). The typical domain size is ~ 30 nm. Each terrace of Au(111) contains multiple domains of 9-AGNRs, indicating several nucleation sites along each terrace. Well-defined domains of planar striped features are sometimes surrounded by ill-defined regions that may indicate adsorption of unreacted material. The width of each striped feature is ~ 1.2 nm, and it is uniform across the surface (Figure 2c,d). This is in good agreement with the expected width of 9-AGNRs estimated

from a molecular mechanics model (Figure 2e) and further indicates that the 9-AGNRs remain parallel (face-on) to the Au(111) surface. The 9-AGNRs appear continuous and close-packed within each domain. While the STM images provided in Figure 2 reveal GNRs with lengths of up to ~20 nm, the length can reach up to 30–35 nm (see Figure S3).

After the growth, the 9-AGNRs can be readily transferred to other substrates, yielding a large-area uniform GNR film, as demonstrated by optical images and Raman mapping (Figure S4). UV–vis–NIR absorption analysis of the 9-AGNRs was carried out by multiple transfer of 9-AGNR films onto one fused silica substrate to have enough optical density (Figure 3a). An absorption onset was thus detectable at ~1185 nm in

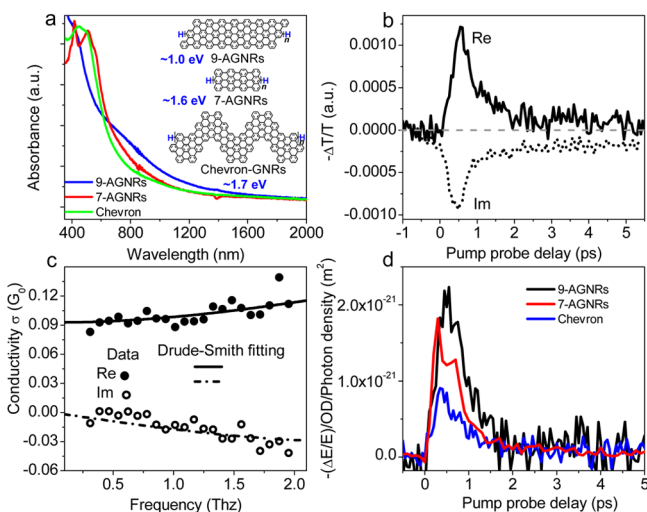


Figure 3. (a) UV–vis–NIR absorption spectra of different CVD-grown GNRs. The inset shows the chemical structures of the GNRs and their optical band gaps. (b) Time-resolved photoinduced real and imaginary conductivities of 9-AGNRs measured as the relative change in terahertz transmission at the peak of the terahertz pulse (real, solid line) and the zero-crossing point of the terahertz pulse (imaginary, dotted line) (pump at 400 nm with a fluence of 200 $\mu\text{J}/\text{cm}^2$). (c) Frequency-resolved terahertz conductivity of 9-AGNRs measured at the peak of the photoconductivity and a Drude–Smith fit with $c \approx -0.72 \pm 0.02$. (d) Comparative study of terahertz photoconductivities of different GNR structures.

the IR region, suggesting an optical band gap of ~1.0 eV for the obtained 9-AGNR multilayer film, which is close to the theoretical value for isolated 9-AGNR¹⁵ and significantly smaller than the values for 7-AGNRs (~1.6 eV) and chevron-type GNRs (~1.7 eV) (see Figures 3a and S5).

To assess the potential of the 9-AGNRs for optoelectronics, we investigated their photoconductivity by OPTP,¹⁹ which has been demonstrated as a powerful spectroscopic tool for contact-free and noninvasive characterization of the intrinsic charge-carrier mobility within individual solution-synthesized GNRs.^{4,5,20} In Figure 3b we show the time-resolved photoconductivity dynamics (in the form of the transient change in the terahertz transmission) of a thin film of 25 layers of 9-AGNRs deposited on fused silica. After photoexcitation with the optical pulse (400 nm wavelength), we observe a subpicosecond rapid rise and a subsequent (~2 ps) fast decay in the real conductivity. The imaginary conductivity displays a similarly fast rise time, but the decay time is considerably longer. Both the transient conductivity dynamics and their time scale are fully consistent with the results of our previous studies

on solution-synthesized GNRs in dispersions^{4,5,20} and can be rationalized by charge-state transitions from quasi-free cases at early times (<1 ps) to strongly bound excitons at longer time delays (>2 ps with a long-lived imaginary conductivity indicative of photoinduced dielectric polarizability of the sample). Furthermore, the frequency-dependent terahertz conductivity at the peak position of the dynamics shown in Figure 3b (~0.55 ps after photoexcitation) is demonstrated in Figure 3c. We observe a positive real component and a negative imaginary component, with both amplitudes increasing with the frequency, sharing a large similarity with the frequency-resolved terahertz conductivity in semiconducting polymers^{21–23} and other types of GNRs dispersed in organic solvents.⁴ The Drude–Smith (DS) model²⁴ has been widely employed to model the transport characteristic in conducting polymers and GNRs as

$$\sigma_{\text{DS}} = \frac{\epsilon_0 \omega_p^2 \tau}{1 - i\omega\tau} \left(1 + \frac{c}{1 - i\omega\tau} \right)$$

where ϵ_0 is the vacuum permittivity, ω_p is the plasma frequency (which is proportional to the carrier concentration), τ is the electron momentum scattering time, and the parameter c accounts for the correlation between the carrier momenta before and after a scattering event, with $c = 0$ as nonpreferential, fully isotropic scattering (classical Drude model of a free electron plasma) and $c = -1$ as the backscattering-dominant process of localized charge carriers. By fitting the complex conductivity using the DS model as shown in Figure 3c, we can obtain $c \approx -0.72 \pm 0.02$, which is fully consistent with previously reported c values in randomly oriented 1D Drude conductors, such as carbon nanotubes and GNRs in dispersions.²⁰ On the basis of the fitting, we can also derive the momentum scattering time to be 20 ± 5 fs. Applying the reported effective mass of 9-AGNRs ($m^* = 0.1 \cdot m_0$),¹⁰ one can readily estimate the intrinsic direct-current carrier mobility in 9-AGNRs using $\mu = e\tau/m^*$, which results in a value of 352 ± 88 $\text{cm}^2 \cdot \text{V}^{-1} \cdot \text{s}^{-1}$. This is a rough estimation of the local carrier mobility within a nanoribbon. The physical length of the molecular wire has been reported to affect its charge mobility because of the charge scattering effect at the ends of the molecular wires.²⁵ Consequently, controlling the growth conditions to produce even longer 9-AGNRs than those reported here (up to ~35 nm) could be beneficial for further boosting the high-frequency carrier mobility of 9-AGNRs for device applications. Speaking of the measured photoconductivity of the sample, we can also estimate the carrier mobility in the film of 25 layers of GNR networks—a film of GNR chains intricately connected with each other. This can be estimated from the average measured conductivity and the quantum efficiency (which in similar materials has been found to be $\text{QE} = 10^{-3} - 10^{-5}$).²² Thus, the mobility in the film is comparable to $50 - 5000$ $\text{cm}^2 \cdot \text{V}^{-1} \cdot \text{s}^{-1}$, which indicates the high quality of the CVD-grown GNRs used in this study. We expect a negligible effect of sample thickness on the mobility estimate for samples consisting of a large number of layers, such as 25 layers in this study (see the Supporting Information for extended discussion). It should be noted that this intrinsic charge-carrier mobility estimated for 9-AGNRs is much higher than the mobility measured in FET devices on thin films of 7-AGNRs and chevron-type GNRs (estimated to be $\sim 10^{-3} - 10^{-5}$ $\text{cm}^2 \cdot \text{V}^{-1} \cdot \text{s}^{-1}$),^{6,12} since the electrical response in the GNR FET devices is mostly dominated by the large inter-GNR junction

resistances as well as the contact resistance between the GNRs and the electrodes.

To establish the potential of 9-AGNRs for optoelectronic applications, we conducted a further comparative investigation of photoconductivity for two other CVD-grown GNRs with certain structural similarities, namely, 7-AGNRs and chevron-type GNRs (see Figure 3a). By selectively exciting the samples with a fixed pump fluence at 400 nm, we compared the photon-induced terahertz conductivities for these three GNR structures, as shown in Figure 3d. As we can see, for a given excitation fluence and optical density (OD), the photoconductivity of 9-AGNRs is a factor of 1.2 and 2.5 higher than those of 7-AGNRs and chevron-type GNRs, respectively, which can be partially attributed to the relatively smaller electron effective mass, leading to a higher mobility, of 9-AGNRs compared with the other GNRs.^{10,26,27}

In summary, a synthesis of structurally well-defined 9-AGNRs has been achieved through a highly efficient CVD method. STM, Raman, UV-vis-NIR absorption, and time-resolved terahertz spectroscopy analyses manifested the high quality of the 9-AGNRs with a low band gap of ~1.0 eV and absorption extending up to ~1200 nm. In view of the scalability and low cost of the CVD synthetic method, these results pave the way for exploiting such bottom-up synthesized GNRs for efficient optoelectronic device applications, including visible-to-infrared photodetectors and photovoltaics.

■ ASSOCIATED CONTENT

Supporting Information

The Supporting Information is available free of charge on the ACS Publications website at DOI: 10.1021/jacs.7b00776.

Experimental details and more characterization data: MALDI-TOF MS data, Raman spectra, and AFM/STM images (PDF)

■ AUTHOR INFORMATION

Corresponding Authors

*narita@mpip-mainz.mpg.de

*bonn@mpip-mainz.mpg.de

*muellen@mpip-mainz.mpg.de

ORCID

Hai I. Wang: 0000-0003-0940-3984

Kunal S. Mali: 0000-0002-9938-6446

Wen Zhang: 0000-0001-8847-1664

Pascal Ruffieux: 0000-0001-5729-5354

Klaus Müllen: 0000-0001-6630-8786

Notes

The authors declare no competing financial interest.

■ ACKNOWLEDGMENTS

This work was financially supported by DFG Priority Program Graphene SPP 1459, the Max Planck Society, the Office of Naval Research BRC Program, the Swiss National Science Foundation, and the European Commission through the FET-Proactive Project “MoQuaS” (FP7-ICT-2013-10, Contract 610449), EU CIG (334324 LIGHTER), and Graphene Flagship.

■ REFERENCES

(1) Yang, L.; Park, C. H.; Son, Y. W.; Cohen, M. L.; Louie, S. G. *Phys. Rev. Lett.* **2007**, *99*, 186801.

(2) Son, Y. W.; Cohen, M. L.; Louie, S. G. *Phys. Rev. Lett.* **2006**, *97*, 216803.

(3) Cai, J. M.; Ruffieux, P.; Jaafar, R.; Bieri, M.; Braun, T.; Blankenburg, S.; Muoth, M.; Seitsonen, A. P.; Saleh, M.; Feng, X. L.; Müllen, K.; Fasel, R. *Nature* **2010**, *466*, 470–473.

(4) Narita, A.; Feng, X.; Hernandez, Y.; Jensen, S. A.; Bonn, M.; Yang, H.; Verzhbitskiy, I. A.; Casiraghi, C.; Hansen, M. R.; Koch, A. H.; Fytas, G.; Ivasenko, O.; Li, B.; Mali, K. S.; Balandina, T.; Mahesh, S.; De Feyter, S.; Müllen, K. *Nat. Chem.* **2014**, *6*, 126–132.

(5) Narita, A.; Verzhbitskiy, I. A.; Frederickx, W.; Mali, K. S.; Jensen, S. A.; Hansen, M. R.; Bonn, M.; De Feyter, S.; Casiraghi, C.; Feng, X.; Müllen, K. *ACS Nano* **2014**, *8*, 11622–11630.

(6) Chen, Z.; Zhang, W.; Palma, C.-A.; Lodi Rizzini, A.; Liu, B.; Abbas, A. N.; Richter, N.; Martini, L.; Wang, X.-Y.; Cavani, N.; Lu, H.; Mishra, N.; Coletti, C.; Berger, R.; Klappenberger, F.; Kläui, M.; Candini, A.; Affronte, M.; Zhou, C.; De Renzi, V.; del Pennino, U.; Barth, J. V.; Räder, H. J.; Narita, A.; Feng, X.; Müllen, K. *J. Am. Chem. Soc.* **2016**, *138*, 15488–15496.

(7) Ruffieux, P.; Wang, S.; Yang, B.; Sánchez-Sánchez, C.; Liu, J.; Diemel, T.; Talirz, L.; Shinde, P.; Pignedoli, C. A.; Passerone, D.; Dumslaff, T.; Feng, X.; Müllen, K.; Fasel, R. *Nature* **2016**, *531*, 489–492.

(8) Sakaguchi, H.; Song, S.; Kojima, T.; Nakae, T. *Nat. Chem.* **2017**, *9*, 57–63.

(9) Narita, A.; Wang, X. Y.; Feng, X. L.; Müllen, K. *Chem. Soc. Rev.* **2015**, *44*, 6616–6643.

(10) Talirz, L.; Ruffieux, P.; Fasel, R. *Adv. Mater.* **2016**, *28*, 6222–6231.

(11) Talirz, L.; Söde, H.; Dumslaff, T.; Wang, S.; Sanchez-Valencia, J. R.; Liu, J.; Shinde, P.; Pignedoli, C. A.; Liang, L.; Meunier, V.; Plumb, N. C.; Shi, M.; Feng, X.; Narita, A.; Müllen, K.; Fasel, R.; Ruffieux, P. *ACS Nano* **2017**, *11*, 1380–1388.

(12) Sakaguchi, H.; Kawagoe, Y.; Hirano, Y.; Iruka, T.; Yano, M.; Nakae, T. *Adv. Mater.* **2014**, *26*, 4134–4138.

(13) Bennett, P. B.; Pedramrazi, Z.; Madani, A.; Chen, Y. C.; de Oteyza, D. G.; Chen, C.; Fischer, F. R.; Crommie, M. F.; Bokor, J. *Appl. Phys. Lett.* **2013**, *103*, 253114.

(14) Shockley, W.; Queisser, H. J. *J. Appl. Phys.* **1961**, *32*, 510–519.

(15) Prezzi, D.; Varsano, D.; Ruini, A.; Marini, A.; Molinari, E. *Phys. Rev. B: Condens. Matter Mater. Phys.* **2008**, *77*, 041404.

(16) Li, G.; Yoon, K.-Y.; Zhong, X.; Zhu, X.; Dong, G. *Chem. - Eur. J.* **2016**, *22*, 9116–9120.

(17) Zhou, J.; Dong, J. *Appl. Phys. Lett.* **2007**, *91*, 173108.

(18) Saito, R.; Furukawa, M.; Dresselhaus, G.; Dresselhaus, M. S. *J. Phys.: Condens. Matter* **2010**, *22*, 334203.

(19) Ulbricht, R.; Hendry, E.; Shan, J.; Heinz, T. F.; Bonn, M. *Rev. Mod. Phys.* **2011**, *83*, 543–586.

(20) Jensen, S. A.; Ulbricht, R.; Narita, A.; Feng, X.; Müllen, K.; Hertel, T.; Turchinovich, D.; Bonn, M. *Nano Lett.* **2013**, *13*, 5925–5930.

(21) Cunningham, P. D.; Hayden, L. M. *J. Phys. Chem. C* **2008**, *112*, 7928–7935.

(22) Hendry, E.; Koeberg, M.; Schins, J. M.; Nienhuys, H. K.; Sundström, V.; Siebbeles, L. D. A.; Bonn, M. *Phys. Rev. B: Condens. Matter Mater. Phys.* **2005**, *71*, 125201.

(23) Hendry, E.; Schins, J. M.; Candeias, L. P.; Siebbeles, L. D. A.; Bonn, M. *Phys. Rev. Lett.* **2004**, *92*, 196601.

(24) Smith, N. V. *Phys. Rev. B: Condens. Matter Mater. Phys.* **2001**, *64*, 155106.

(25) Prins, P.; Grozema, F. C.; Schins, J. M.; Patil, S.; Scherf, U.; Siebbeles, L. D. A. *Phys. Rev. Lett.* **2006**, *96*, 146601.

(26) Raza, H.; Kan, E. C. *Phys. Rev. B: Condens. Matter Mater. Phys.* **2008**, *77*, 245434.

(27) Bronner, C.; Haase, A.; Tegeder, P. *Phys. Rev. B: Condens. Matter Mater. Phys.* **2015**, *91*, 045428.